Transient Analysis of Coupling Between Crossing Lines in Three-Dimensional Space

SHOICHI KOIKE, NORINOBU YOSHIDA, AND ICHIRO FUKAI

Abstract—**Coupling of crossing lines has not been studied extensively since it is very complicated and difficult to estimate. But recently with the development of high density wiring and large-scale integration rigorous analysis of coupling effects has become more important. In this analysis not only the electric and magnetic fields but also the Poynting vector are important. Especially, the variation of the spatial pattern of the Poynting vector in the time domain clarifies the dynamic coupling characteristics. In this paper the fundamental phenomena of coupling are demonstrated by considering the time variation of the distribution of the Poynting vector and the magnetic and electric fields for a Gaussian pulse in three-dimensional space.**

I. Introduction

Recently the development of high density wiring and the large-scale integration of parts in printed boards or the interconnecting bus demand a rigorous analysis of the coupling effect between crossing lines. At high frequencies, the distributed nature of the circuits must be considered in the analysis. For example, the analysis of the coupling between crossing lines in multilayered wiring is important [1] but difficult because the structure is three dimensional. Conventionally many coupling problems have been treated by introducing coupling capacitances and mutual inductances derived by static field analysis [2]–[6], but the electric and magnetic fields always coexist in the wave and together constitute the Poynting vector. On the other hand, the coupling characteristics may be described in terms of power flow from one line to the other. This property is expressed as the variation of the spatial distribution of the Poynting vector in the time domain. For a complex wiring structure, the propagating electromagnetic wave varies in a very complicated way. All electromagnetic components appear and together give rise to the Poynting vector, i.e., the power flow. Hence a rigorous analysis of the coupling characteristics of the crossing lines demands a three-dimensional vector analysis. Also, the recent development of high-speed pulse techniques requires analysis in the time domain. Hence we have proposed a procedure involving nodal equations that formulate the wave propagation by the Bergeron method [9]–[11]. (This is referred to as the present method.) This method uses all electromagnetic field components, and the boundary and medium conditions are represented by the equivalent circuits. Therefore the present method is useful for the formulation of the problem described above in which a complicated boundary shape of the wiring structure exists.

In the present paper two cases of crossing, namely at 45 and 90 degrees, are studied. One of the lines on the dielectric substrate is called the main line and the other line in the dielectric substrate is called the secondary line. Coupling characteristics to the secondary line from the main line are described by time variations of the Poynting vector, the magnetic and electric fields for a pulse wave. The effect by the crossing angle also is clarified.

Manuscript received November 27, 1985; revised July 24, 1986

The authors are with the Department of Electrical Engineering, Faculty of Engineering, Hokkaido University, Sapparo 060, Japan.

IEEE Log Number 8611394.

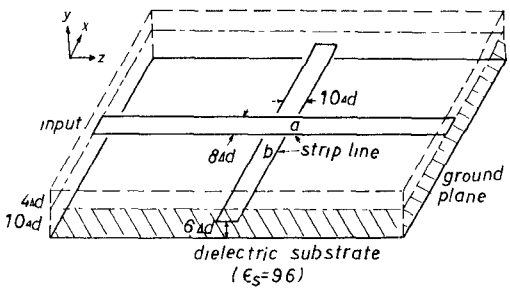

Fig. 1. Model of the crossing microstrip lines.

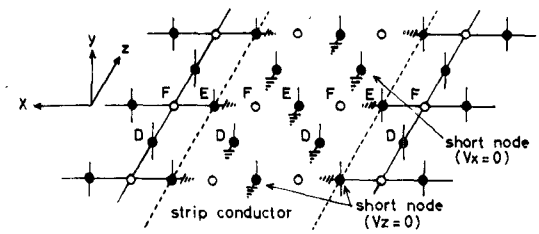

Fig. 2. Arrangement of nodes on the plane including the stripline.

II. Treatment of Crossing Microstrip Lines in Three-Dimensional Space

By means of the equivalent circuit of the electromagnetic field, the nodal equations for the electromagnetic field including the complex boundary and medium conditions are derived. In Fig. 1, the model of the crossing microstrip line is shown. In this figure, Δd is the interval between adjacent nodes in the equivalent circuit. In order to model this structure by the present method three principal conditions are introduced, namely the boundary condition at the conductor, the boundary condition at the free boundary which is the surface of the analyzed region, and the condition of the dielectric. In this paper we do not give the details of these formulations, but the boundary condition at the conductor is explained in detail because it is important in the formulation.

The conductor is assumed to have infinite conductivity so that the tangential components of the electric field and the normal components of the magnetic field on the surface of the conductor are zero. For example, the equivalent circuit of the planes including the stripline in Fig. 1 is presented in Fig. 2. Since the coordinate system is as shown in Fig. 1, the surface of the conductor is situated in the xz-plane. As shown in Fig. 2, the xz-plane is identified as DFE (consisting only of nodes D, F, and E) surface. In this figure, the notations ● and ○ represent the electric node in which the voltage variable corresponds to the electric-field component and the magnetic node in which the voltage variable corresponds to the magnetic-field component, respectively. Fig. 2 shows the resultant equivalent circuit of the planes including the stripline. The details of the correspondence between the equivalent circuit variables and the electromagnetic variables are shown in [9, Table I]. For example, at the D or E nodes on the surface of the conductor, the nodes are short-circuited because the voltage corresponds to the tangential component of the electric field, namely E_x and E_z, which are both equal to zero. Therefore, the upper and lower surfaces of the conductor

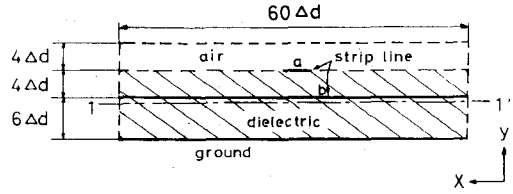

Fig. 3. x-y cross section of the crossing striplines.

are separated. F nodes are neglected because currents and voltage at these nodes correspond to the field component E_x, E_z, and H_y, respectively, all of which are equal to zero on the surface of the conductor.

III. Results of the Analysis and Discussion

In this section we present the time variation of the electromagnetic field for the Gaussian pulse. These results are shown in the form of the Poynting vector diagram, the magnetic-field diagram, and the amplitude distribution of the electric field at the observation plane 1-1′ in Fig. 3, which shows the x-y section of the analyzed region. The input condition of the Gaussian pulse gives the transient characteristics of the coupling of the electromagnetic field between lines in the time domain. The mechanism of the coupling is clarified by the spatial and time variations of each electromagnetic-field component. The analysis is performed for two configurations of lines, crossing each other at 90 and 45 degrees, respectively. In order to observe the propagation of the induced wave along the secondary line b, the observation plane is situated $1\Delta d$ beneath the secondary line. The time waveform of the Gaussian pulse is assumed as follows:

$$G(t) = \exp\left\{-\alpha(t-t_0)^2\right\}, \qquad \alpha = (\pi/T)^2. \tag{1}$$

In the analysis, the initial time $t=0$ is the time at which the amplitude of the input pulse has reached 1/10 of its peak value. Furthermore, the time interval T is $240\Delta t$, where Δt is the time interval between iterations and corresponds to the propagation time between adjacent nodes in the equivalent circuit. When $1\Delta d$ is assumed to be 1.0 mm, the time interval T corresponds to 0.4 ns. The dielectric constant of the substrate is 9.6.

A. Poynting Vector Diagram

For 90 Degrees Crossing Angle: The time variation of the instantaneous Poynting vector for a Gaussian pulse incident on the main line a in Fig. 1 is shown in Fig. 4. In the figures, the length and the direction of the arrows correspond to the magnitude and the direction of the Poynting vector, respectively. For clarity the length of the arrows is normalized to the maximum value in each observed time interval. The value is noted in each figure, and all arrows shorter than one five-hundredth of the maximum value in Fig. 4(a) are omitted. In Fig. 4(a), it appears that the applied electromagnetic wave propagates radially. The power flow is concentrated under the main line but spreads considerably sideways. We call these concentrated groups of arrows a "crowd". The crowd propagates in the z-direction and follows the main line. In Fig. 4(b), the crowd has reached the crossing region of the lines, and the Poynting vector component in the z-direction is dominant. However, a Poynting vector component in the x-direction begins to appear near the secondary line b. In Fig. 4(c), the main crowd has passed over the crossing region in the main line. The small fragment of the crowd in the incident part of the main line is the reflected crowd from

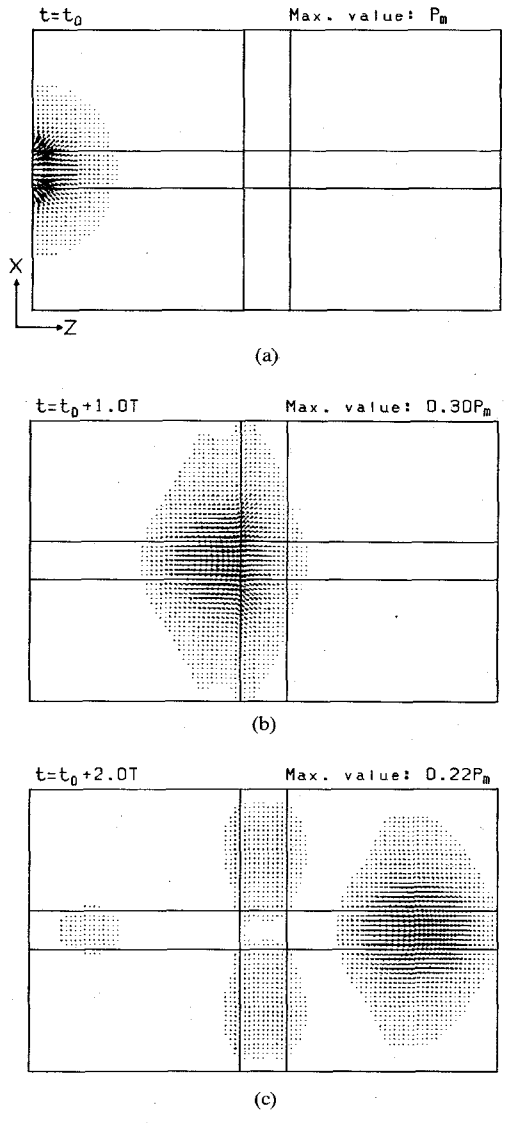

Fig. 4. Time variation of the instantaneous Poynting vector for a crossing angle of 90 degrees.

the crossing part. A small fragment of the crowd propagating along the secondary line in the x-direction also appears. Its magnitude corresponds to the coupling characteristics between the main line and the secondary line. In this case, as the crossing angle is 90 degrees, the analyzed region is symmetrical about the center axis of the main line a. Hence, Fig. 4(a)–(c) shows a symmetrical distribution of the Poynting vector. The spatial pattern of the crowd of the Poynting vector shows that the propagation of the pulse wave is fundamentally guided by the stripline, but the region in which the energy concentrates spreads considerably beyond the side of the stripline. These properties affect the coupling characteristics. The maximum magnitude of the Poynting vector in each crowd, in the incident, output, and secondary lines in Fig. 4(c) are about -20.0, -1.4, and -11.0 dB, respectively. These values are evaluated from the ratio of each maximum value of the crowds in Fig. 4(c) to maximum value in Fig. 4(b). These values give information on the characteristics of the reflected wave, the insertion loss, and the coupled wave in the steady state.

For 45 Degrees Crossing Angle: Fig. 5 shows the time variation of the Poynting vector when the secondary line b crosses the

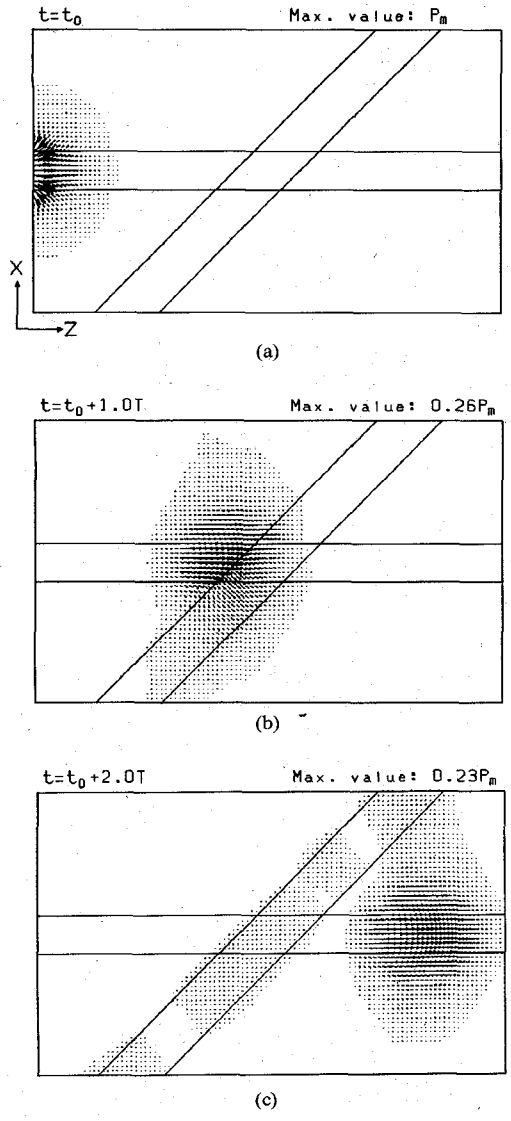

Fig. 5. Time variation of the instantaneous Poynting vector for a crossing angle of 45 degrees.

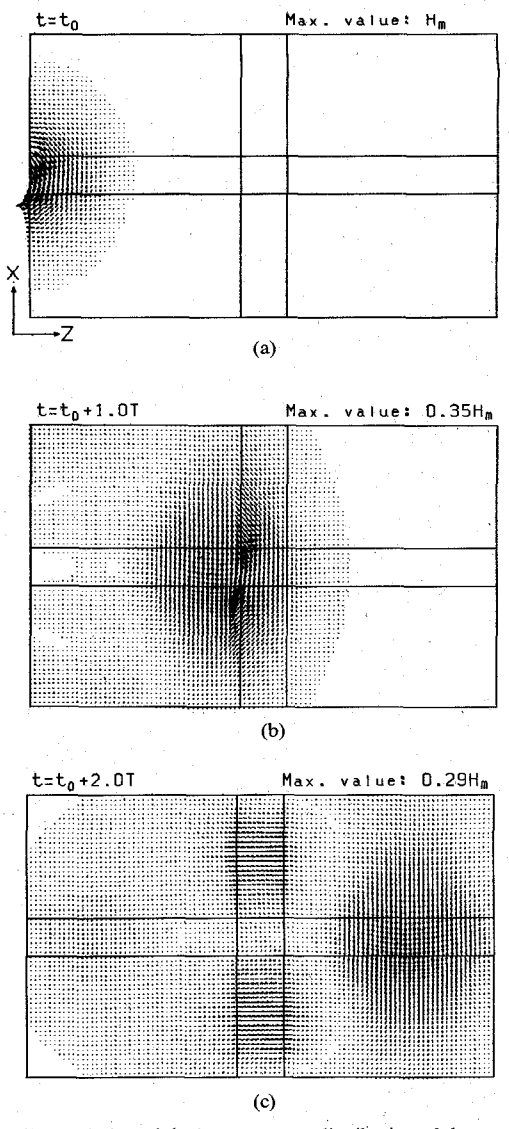

Fig. 6. Time variation of the instantaneous distribution of the magnetic field for a crossing angle of 90 degrees.

main line a at an angle of 45 degrees. The position of the observation plane, the input condition, and the line widths are the same as in the former case. The distribution of the Poynting vector in Fig. 5(a) is the same as in Fig. 4(a) because the electromagnetic wave has not yet reached the crossing region. In Fig. 5(b), the electromagnetic wave has reached the crossing region, and the crowd of the pulse has reached the left lower part of the secondary line before reaching its right upper part, but the shape of the crowd does not change distinctly. It appears that the Poynting vector enters the secondary line perpendicularly. In Fig. 5(c), the main crowd has passed over the crossing region. The wave induced on the secondary line b propagates in the upper right and lower left directions. In this time of observation, part of the main crowd is still interacting with the secondary line on its right upper side. The crowd caused by reflection at the crossing does not appear on the left of the main line as shown in Fig. 4(c). Considering the spread of the crowd along the secondary line b, the coupling for the crossing angle of 45 degrees is greater than that for the case of 90 degrees. But in both cases the electromagnetic wave propagating along the main line is dominant, and the coupled wave on the secondary line b is small compared with the crowd in the main line. On the other hand, the reflection on the left side of the main line is greater for the crossing angle 90 degrees than for the case of 45 degrees. The maximum magnitude of the Poynting vector in each crowd, in the output side and the secondary line in Fig. 5 are about -1.10 and -11.7 dB, respectively. The latter value is almost the same as that for 90 degrees, but the crowd spreads along the secondary line so the total coupling in this case is larger than that for 90 degrees.

B. *Variation of the Magnetic Field*

For 90 Degrees Crossing Angle: Fig. 6 shows the time variation of the instantaneous magnetic field when the crossing angle is 90 degrees. The length and the direction of arrows correspond to the magnitude and the direction of the magnetic field, respectively. The normalization is done in the same way as in the previous case. The rotation of the magnetic field at the crossing part appears clearly and determines the directions of the induced wave in the secondary line propagating in the upper and lower directions. The magnetic field in Figs. 6 and 7 and the electric field E_y in Figs. 8 and 9 produce the Poynting vector in the observation plane. Compared with figures for the Poynting vector

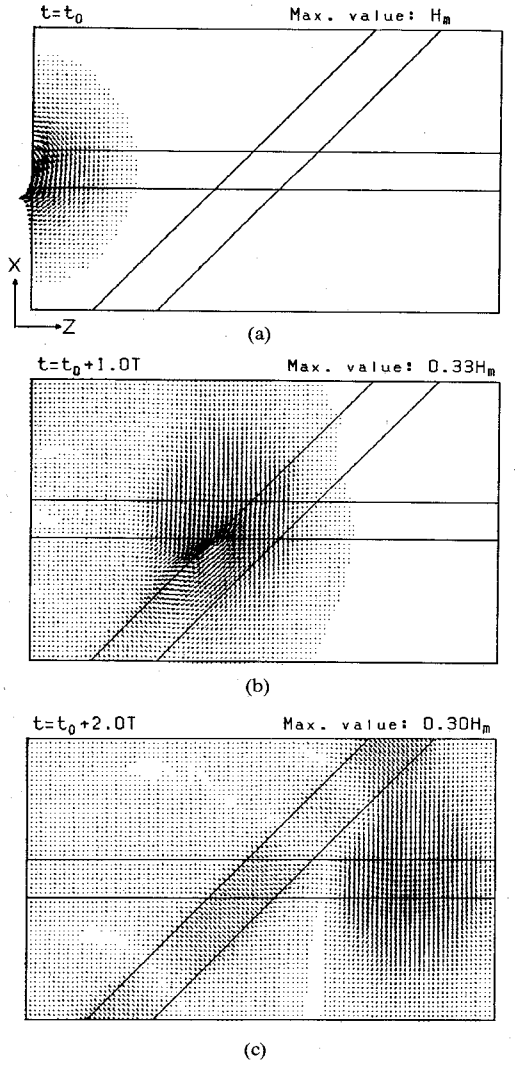

Fig. 7. Time variation of the instantaneous distribution of the magnetic field for a crossing angle of 45 degrees.

the distribution of the magnetic field spreads over a larger area. The higher spatial concentration of the Poynting vector is caused by the product of the electric and magnetic fields.

For 45 Degrees Crossing Angle: Fig. 7 shows the time variation of the instantaneous magnetic field when the crossing angle is 45 degrees. Compared to Fig. 6, Fig. 7(a) is similar to Fig. 6(a); the other figures differ because of the differences in the crossing angle. The rotation of the magnetic field at the crossing appears distinctly and this determines the directions of the induced wave in the secondary line.

C. Transient Electric-Field Distribution

For 90 Degrees Crossing Angle: Fig. 8 shows the time variation of instantaneous values of the electric field E_y for a crossing angle of 90 degrees. The observed plane is the same as in Figs. 4–7. The amplitude in each figure is normalized to the maximum value at time $t = t_0$ for ease of viewing. In Fig. 8(a), the electric field E_y is maximum at the axis and distributes symmetrically about the axis of the main line. In Fig. 8(b), the front of the wave seems to be cut by the secondary line b. The edge effect does not appear in the wave propagating along the main line a, but it appears in the wave propagating along the secondary line b. These conditions occur because the xz-plane in which we observe

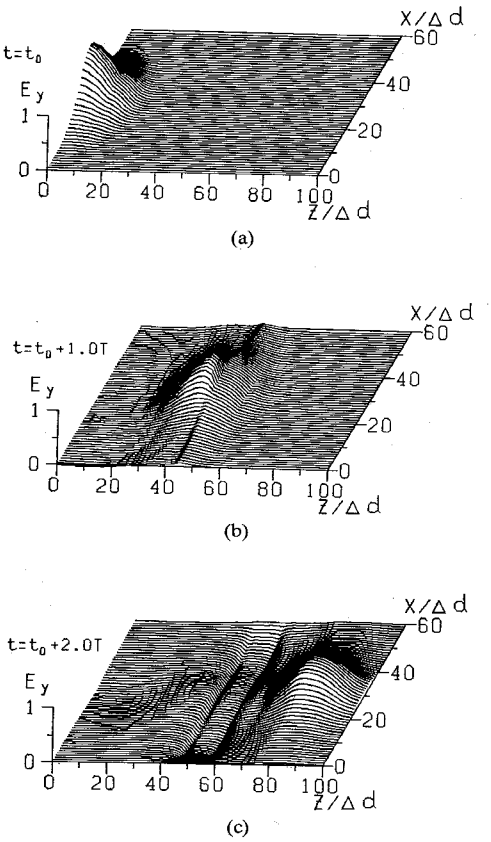

Fig. 8. Time variation of the instantaneous distribution of the electric field E_y for a crossing angle of 90 degrees.

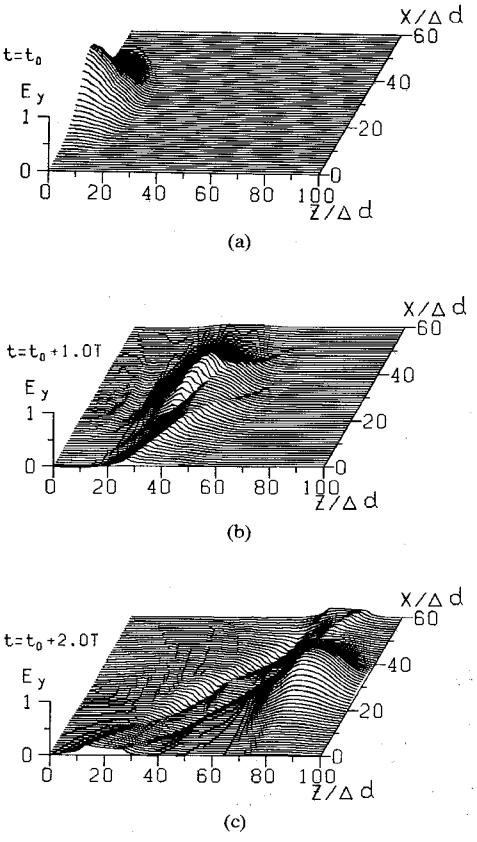

Fig. 9. Time variation of the instantaneous distribution of the electric field E_y for a crossing angle of 45 degrees.

is situated $5\Delta d$ beneath the main line a and $1\Delta d$ beneath the secondary line b. If the plane of observation is nearer the main line a, the edge effect along the main line a will appear clearly. In Fig. 8(c), the main wave has passed over the crossing region. The wave reflected from the crossing appears on the left part of the secondary line b. The wave has the opposite phase because of the reflection by the conductor, but its magnitude is very small. The characteristics of these figures relate to the Poynting vector in Fig. 4 and the magnetic field in Fig. 6. The spatial spread of the distribution of the electric field E_y is not as wide as that of the magnetic field.

For 45 Degrees Crossing Angle: Fig. 9 shows the instantaneous time variation of the electric field E_y for the crossing angle of 45 degrees. Fig. 9(a) is the same as Fig. 8(a) because the wave has not reached the crossing area in both cases. Comparing Fig. 9(b) and (c) with Fig. 8(b) and (c), it is observed that the coupling characteristics of the 45 degrees case is more complicated than that of 90 degrees. This is caused by the different coupling process of each part of the crowd to the secondary line in space and time.

IV. Conclusions

In this paper the coupling between two crossing lines is described qualitatively. It is noted that the spatial spread of the fields of the propagating wave about the line causes complicated coupling characteristics. This also has importance in the analysis of the coupling characteristics of other configurations of lines, such as parallel lines. The quantitative evaluation of various coupling parameters is being studied now, and the results will be reported in a later paper. The importance of the Poynting vector corresponding to the power flow in the coupling characteristics should be investigated more rigorously. The coupling of more complex line configurations may be treated by the present method.

References

[1] D. V. Giri, S.-K. Chang, and F. M. Tesche, "A coupling model for a pair of skewed transmission lines," *IEEE Trans. Electromagn. Compat.*, vol. EMC-22, pp. 20–28, Feb. 1980.

[2] T. G. Bryant and J. A. Weiss, "Parameters of microstrip transmission lines and of coupled pairs of microstrip lines," *IEEE Trans. Microwave Theory Tech.*, vol. MTT-16, pp. 1021–1027, Dec. 1968.

[3] C. R. Paul and A. E. Feather, "Computation of the transmission line inductance and capacitance matrices from the generalized capacitance matrix," *IEEE Trans. Electromagn. Compat.*, vol. EMC-18, pp. 175–182, Nov. 1976.

[4] A. K. Agrawal, H. J. Price, and S. H. Gurbaxani, "Transient response of multiconductor transmission lines excited by a nonuniform electromagnetic field," *IEEE Trans. Electromagn. Compat.*, vol. EMC-22, pp. 119–129, May 1980.

[5] Y. Kami and R. Sato, "Equivalent circuit for transmission lines excited by external electromagnetic waves," *Trans. IECE Japan*, vol. J66-B, pp. 687–688, May 1983.

[6] N. Schibuya, H. Takagi, K. Kumamoto, T. Homma, and K. Ito, "Crosstalk noise analysis of wiring on the printed circuit board," *Trans. IECE Japan*, vol. J68-B, pp. 1068–1076, Sept. 1985.

[7] S. Koike, N. Yoshida and I. Fukai, "Transient analysis of microstrip gap in three-dimensional space," *IEEE Trans. Microwave Theory Tech.*, vol. MTT-33, pp. 726–730, Aug. 1985.

[8] S. Koike, N. Yoshida, and I. Fukai, "Transient analysis of directional coupler using coupled microstrip-slot-line in three-dimensional space," *IEEE Trans. Microwave Theory Tech.*, vol. MTT-34, pp. 353–357, Mar. 86.

[9] N. Yoshida and I. Fukai, "Transient analysis of a stripline having a corner in three-dimensional space," *IEEE Trans. Microwave Theory Tech.*, vol. MTT-32, pp. 491–498, May 1984.

[10] S. Koike, N. Yoshida, and I. Fukai, "Transient analysis of microstrip gap," *Trans. IECE Japan*, vol. J67-B, pp. 662–669, June 1984.

[11] S. Koide, N. Yoshida, and I. Fukai, "Transient analysis of coupled microstrip-slot-line," *Trans. IECE Japan*, vol. J68-B, pp. 811–818, July 1985.

A Method for Measurement of Losses in the Noise-Matching Microwave Network While Measuring Transistor Noise Parameters

GIOVANNI MARTINES AND MARIO SANNINO

Abstract **— A new method for measuring the loss of a tuner network used as the noise-source admittance transformer in a noise parameter test set is presented. Since the method is based on noise figure measurements, the tuner losses are determined on-line while performing measurements for determining transistor noise parameters.**

Experiments carried out on a coaxial slide-screw tuner by means of a computer-assisted measurement setup are reported.

I. Introduction

Modern techniques for the determination of the four noise parameters which characterize the noise behavior of microwave transistors, i.e., minimum noise figure, optimum reflection coefficient of the input termination (magnitude and phase), and noise resistance, require measurements of the noise figure $F(\Gamma_s)$ of the transistor under test for some (redundant, i.e., more than four) values of the reflection coefficients Γ_s of its input termination. These measurements are made in conjunction with a computer-aided data-processing procedure based on the least-squares method [1]. This procedure furnishes good results, provided that, in selecting the values Γ_s, well-established criteria are followed [2], [3].

The same procedure yields the four available gain parameters of the transistor under test after carrying out measurements of transistor power gain $G_a(\Gamma_s)$ for some (redundant) Γ_s through a gain-measuring setup [1]. These parameters and the scattering parameters can also be derived when determining transistor noise parameters if a proper experimental procedure for measuring $F(\Gamma_s)$ is followed [4]–[7].

The essential component of the noise-parameter-measuring setup is a coaxial or waveguide double-stub or slide-screw tuner inserted between the noise source and the device under test (DUT), in order to transform the noise source reflection coefficient Γ_{ns} to the desired value Γ_s of the DUT input termination. The DUT output noise powers are then detected, through a receiver, by a meter which measures the noises figure F_m of the whole measuring setup. This figure is given by Friis's formula for cascaded networks, i.e.

$$F_m(\Gamma_{ns}) = \alpha_{\Gamma_s}(\Gamma_{ns})\left(F(\Gamma_s) + \frac{F_r(S'_{22}) - 1}{G_a(\Gamma_s)} \right) \qquad (1)$$

where α_{Γ_s} represents the tuner loss, which depends on the tuner configuration; F, G_a, and S'_{22} are the noise figure, the available power gain, and the output reflection coefficient of the DUT, respectively; and F_r is the receiver noise figure.

From (1), it appears that in order to determine $F(\Gamma_s)$ from the measured noise figure F_m, previous measurements of the tuner loss $\alpha_{\Gamma_s}(\Gamma_{ns})$ are needed. Very little has appeared so far in the literature concerning this measurement.

Manuscript received December 9, 1985; revised August 7, 1986. This work was supported in part by Italian Research Council-Electronic Components, Circuits and Technologies (CCTE) Group and Ministry of Education.

The authors are with the Dipartimento di Ingegneria Elettrica, Universita di Palermo, Viale delle Scienze, Palermo, Italy.

IEEE Log Number 8611025.